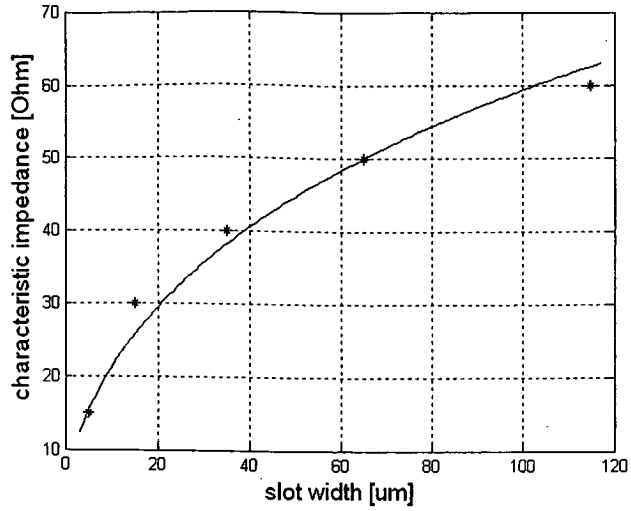

Figure 3 Characteristic impedance vs. slot width: —— simulated results; * reference [8]

$$C = C_0 + C_1 + C_{thin}, \tag{7}$$

where C_0 is the capacitance per unit for CPWs in the free space, C_1 for the single-layer substrate with relative dielectric constant $(\varepsilon_{r1} - 1)$ and thickness $(h_1 + h_2)$, and C_{thin} for the single-layer substrate with relative dielectric constant $(\varepsilon_{r2} - \varepsilon_{r1})$ and small thickness h_1. The expressions C_0 and C_1 can be obtained from Eqs. 4 and 5 in [1].

Utilizing the effective dielectric constant for CPWs on double-layered substrate $\varepsilon_{eff} = C/C_0$, the characteristic impedance can be obtained as follows:

$$Z = \frac{1}{vC_0\sqrt{\varepsilon_{eff}}}, \tag{8}$$

where v is wave velocity. If the skin effect and the thickness of conductor are considered, the revised sizes [7, 8] are given by

$$t_m = t - \delta, \quad s_m = s - 0.5\delta, \quad g_m = g + \delta, \tag{9}$$

$$s_{eq} = s_m + \frac{t_m}{\pi}, \quad g_{eq} = g_m - \frac{2t_m}{\pi}, \quad w_{eq} \approx w, \tag{10}$$

the skin depth is $\delta = 1/\sqrt{\pi f \mu \sigma}$, where σ is conductivity of conductor. Let $f = 60$ GHz. The characteristic impedance of the CPWs as a function of slot width is shown in Figure 3 and compared with the experiment results in [6]. It can be observed that the results are in good agreement.

REFERENCES

1. C. Veyres and V.F. Hanna, Extension of the application of conformal mapping techniques to coplanar lines with finite dimensions, Int J Electron 48 (1980), 47–56.
2. E. Carlsson and S. Gevorgian, Conformal mapping of the field and change distributions in multilayered substrate CPWs, IEEE Trans Microwave Theory Tech 47 (1999), 1544–1552.
3. L.H. Howell and L.N. Trefethen, A modified Schwarz–Christoffel transformation for elongated regions, Siam J Sci Stat Comput 11 (1990), 928–949.
4. M. Goano, F. Bertazzi, P. Caravelli, G. Ghione, and T.A. Driscoll, A general conformal-mapping approach to the optimum electrode design of coplanar waveguides with arbitrary cross section, IEEE Trans Microwave Theory Tech 49 (2001), 1573–1580.
5. M. Abramowitz and I. Stegun, Handbook of mathematical functions, National Bureau of Standards, 1964.
6. M. Tanabe, M. Nishituji, Y. Anda, and Y. Ota, A low-impedance coplanar waveguide using an SrTiO3 thin film for GaAs power MMICs, IEEE Trans Microwave Theory Tech 48 (2000), 872–874.
7. H.A. Wheeler, Transmission-line properties of a strip on a dielectric sheet on a plane, IEEE Trans Microwave Theory Tech 25 (1977), 631–647.
8. G. Ghione, A CAD-oriented analytical model for the losses of general asymmetric coplanar lines in hybrid and monolithic MICs, IEEE Trans Microwave Theory Tech 41 (1993), 1499–1510.

A K-BAND INVERTED MICROSTRIPLINE-FED LINEAR TAPERED SLOT ANTENNA AND ITS 16-ELEMENT E-PLANE ARRAY

Chen Wu
Defense Research and Development Canada—Ottawa
3701 Carling Ave.
Ottawa, Canada, K1A 0Z4

Received 15 October 2004

ABSTRACT: *An inverted microstripline-fed linear tapered slot antenna element and a design of its 16-element E-plane array are presented in this paper. The element is designed using the finite-difference time-domain (FDTD) method. The calculated results show that it has a wide-impedance bandwidth in the K-band. To investigate the E-plane array, the return loss at each element input port, the couplings among elements, and the array's radiation patterns are obtained using the FDTD method. Using a unique three-piece assembled structure, the array is fabricated and tested experimentally. The measured results show that it has a wide bandwidth and antenna efficiency.* © 2005 Wiley Periodicals, Inc. Microwave Opt Technol Lett 45: 241–246, 2005; Published online in Wiley InterScience (www.interscience.wiley.com). DOI 10.1002/mop.20784

Key words: *microstrip antenna; linear tapered slot antenna; inverted microstrip line; finite-different time-domain method; E-plane array*

1. INTRODUCTION

Although a microstrip-to-slot transition is one of the simplest feeding structures to feed a linear tapered slot antenna (LTSA) [1, 2], the loss in microstripline beam-forming networks (BFNs) is always a major concern, when an array is designed in millimeter or submillimeter-wave frequency bands. To reduce the loss in an array BFN and at the same time use low-cost substrate, the microstripline can be replaced by an inverted microstripline (IML) or a suspended microstripline (SML). These lines usually have lower loss than microstripline [3], because a greater portion of the fields exists the air slab. In [4], an SML-fed LTSA element and a five-piece assembled structure to build an E-plane array were introduced. The drawbacks of the five-piece assembly design are: (i) the LTSA element and the SML BFN are printed on two different printed circuit boards (PCBs); (ii) the structure is difficult to assemble, since a good alignment is needed between the SML and the feeding slot in an LTSA; and (iii) the cost of the array is high, since five components have to be made and assembled. To simplify the design, reduce the cost, and keep low loss in the BFN, an IML-fed LTSA is designed using the FDTD method. A three-

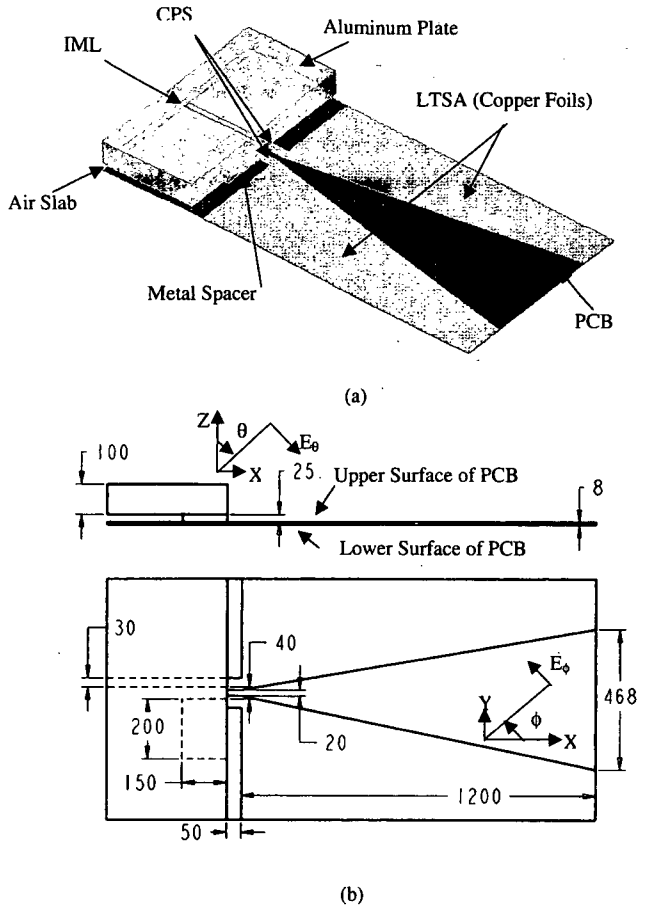

Figure 1 (a) The 3D view and (b) dimensions of the IML-fed LTSA (unit in mil)

piece assembled structure has been created to build the IML-fed LTSA E-plane array. This structure not only retains all the advantages of the SML-fed LTSA E-plane array, but also overcomes the disadvantages of the five-piece assembled structure. The new features are as follows: (i) the radiating element and IML can be printed on the same side of a PCB, (ii) the alignment pins are eliminated, (iii) it can be easily assembled, and (iv) the cost of the array is reduced. To demonstrate the advantages of the three-piece antenna structure, an IML-fed 16-element E-plane array is designed using the FDTD method. The return loss of each element and couplings among elements are investigated. Finally, the three-piece assembled IML-fed 16-element E-plane array is fabricated and tested experimentally. The measured results indicate that the array has a good antenna performance from 17.7 to 23.6 GHz.

2. IML-FED LTSA ELEMENT

A 3D view of the IML-fed LTSA is shown in Figure 1(a). It has an aluminum plate, a PCB, and a metal spacer. The aluminum plate provides a support to the antenna structure, and provides a ground plane for the IML. The metal spacer forms an air slab between the ground plate and the PCB. The IML and the LTSA are printed on the upper surface of the PCB, which is a Rogers RO4003 substrate. Two printed copper foils form the V-slot in the LTSA. To feed the V-slot, one copper foil is directly connected to the IML, and the other one is terminated by the metal spacer, which connects to the ground plate. Between the IML and V-slot, there is a short segment of coplanar strip (CPS) [5]. It provides an impedance matching mechanism between the IML and the V-slot. All the dimensions are given in detail in Figure 1(b). It must be mentioned that an SML-fed LTSA can also be designed using the same approach. Since the SML and the LTSA will be printed on the lower surface of the PCB, extra care must be exercised to make sure that one of the LTSA copper foil is connected to the ground.

Prior to designing the element, the IML-to-CPS transition is optimized using the FDTD method. By changing the spacing between two strips, the width of strips, and the gap between the IML and metal spacer [Fig. 2(a)], a good return loss is obtained at the IML port in a very wide frequency band [Fig. 2(b)]. Figure 1(b) demonstrates that the spacing between two strips is 20 mil, the strip width is 50 mil, and the gap between the IML and the metal spacer is 40 mil. After the transition is optimized, the element is simulated using the FDTD method. The computational domain of the FDTD method is a rectangular box, and the cell numbers are 355, 237, and 80 in the X, Y, and Z directions. Nonuniform grids are used, and the maximum ratio between adjacent grids is 1.25. The size of majority cells is an $8 \times 8 \times 8$-mil cube. Staircasings are used to approximate the linear tapered slot, as shown in Figure

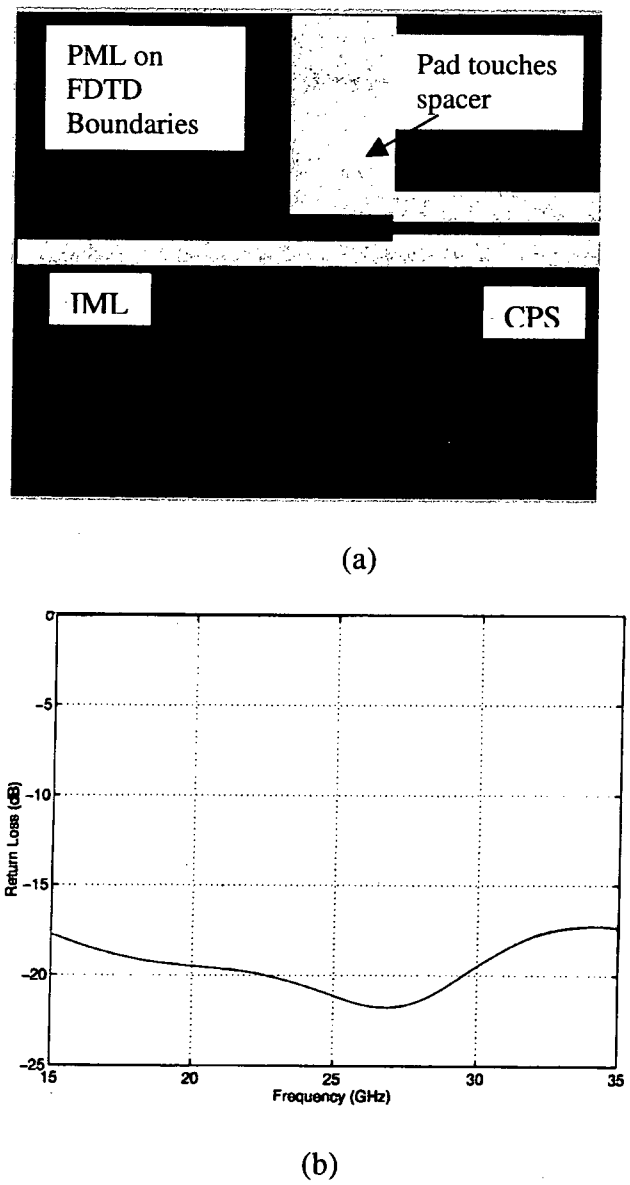

Figure 2 (a) The IML-to-CPS transition and (b) the return loss of the IML-to-CPS transition

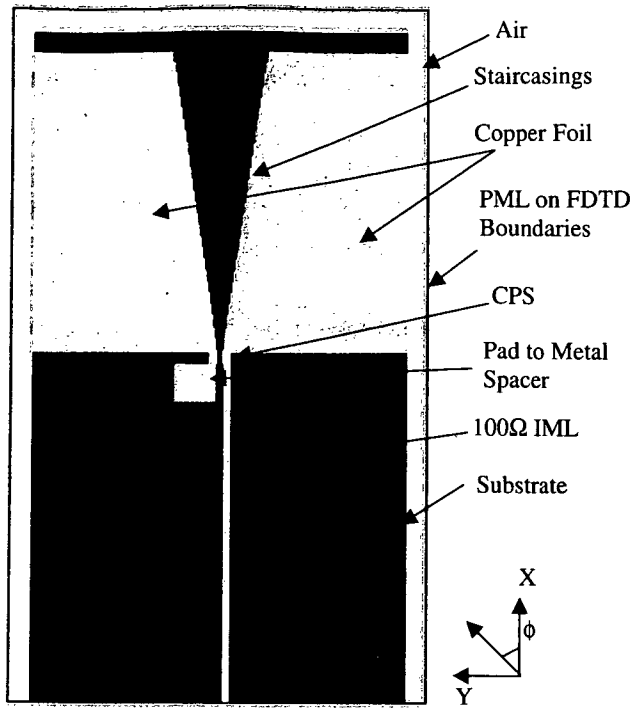

Figure 3 The IML-fed LTSA in a 3D-structure FDTD simulator

3. The simulated return loss at the IML port is given in Figure 4. It is obvious that the element has good return loss from 17.7 to 23.6 GHz, which is a frequency band used for point-to-multipoint communications. It has to be mentioned that the characteristic impedance of the IML is 100Ω. The reasons of choosing a 100Ω line are that the input impedance of the LTSA is about 92Ω [6], and the IML T-junction used in the IML parallel feeding network has a 50Ω input port and two 100Ω output ports. Thus, the output ports of the last stage T-junctions in the BFN can feed the LTSA element directly.

3. 16-ELEMENT E-PLANE ARRAY

Using the element introduced in prior section, the 16-element E-plane array shown in Figure 5 is modeled and studied using the FDTD method. In the model, each element can be excited independently, so the return loss at each element input port and couplings in the E-plane array can be calculated. The procedure for calculating the return losses and couplings in the array is given as follows. A Gaussian pulse excites the i^{th} element, and matched loads terminate rest elements. During the FDTD simulation, time-domain voltage signals are collected at each port of the element.

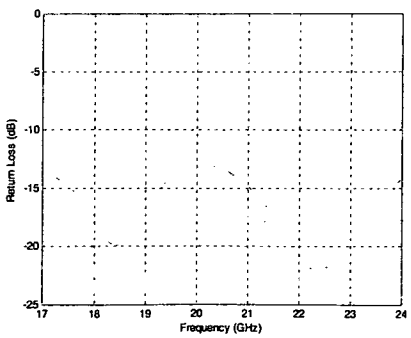

Figure 4 Simulated return loss of the standalone element

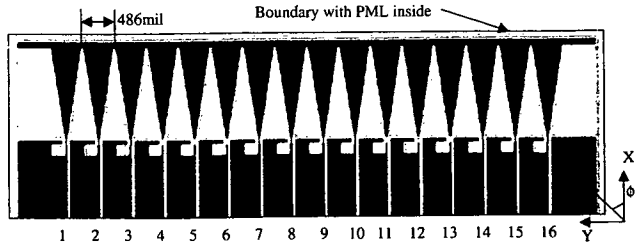

Figure 5 The 16 elements of the LTSA simulated using the FDTD method

Using Fourier transform, the frequency-domain voltages can be obtained and the S-parameters can be calculated using

$$S_{j,i}(f) = \frac{V_{j\,out}(f)}{V_{i\,inc}(f)}, \tag{1}$$

where $V_{i\,inc}(f)$ is the incident wave at the i^{th} port, and $V_{j\,out}(f)$ is the output wave at the j^{th} port ($j = 1, 2, \cdots 16$). When j equals i, $V_{i\,out}(f)$ is the reflected wave from the excitation port. Thus, the return loss of the i^{th} element can be calculated from $S_{i,i}(f)$, and the mutual couplings among elements are given by $S_{j,i}(f)$. Figure 6 shows the return losses of the four elements ($i = 1, 2, 4$, and 8) denoted by solid lines, and the couplings among the elements by dashed and dotted lines. The dashed lines give the coupling between the i^{th} element and the $(i \pm 1)^{th}$ elements, and the dotted lines depict the coupling from the i^{th} element to the ($i \pm$

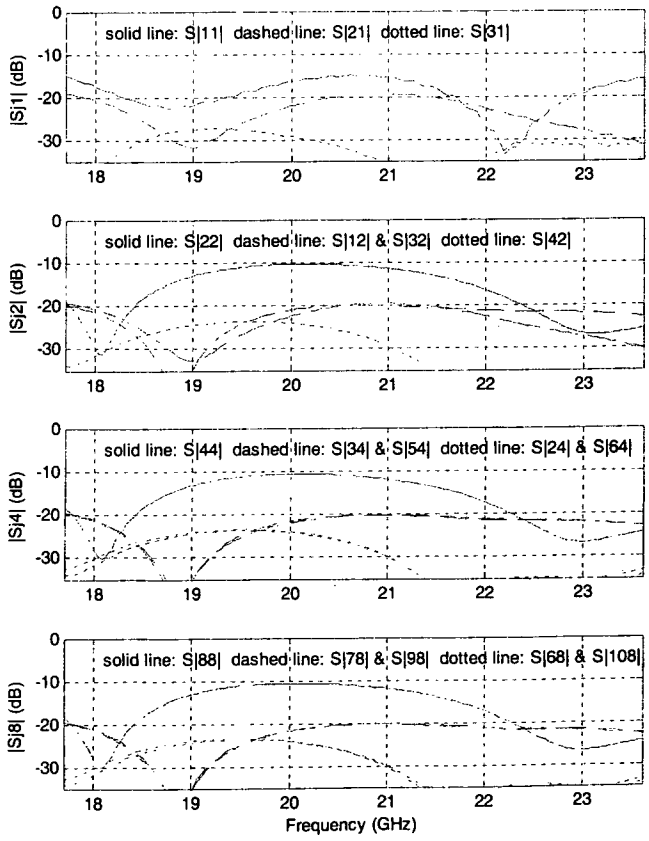

Figure 6 Return losses and mutual couplings when elements 1, 2, 4, and 8 are excited individually

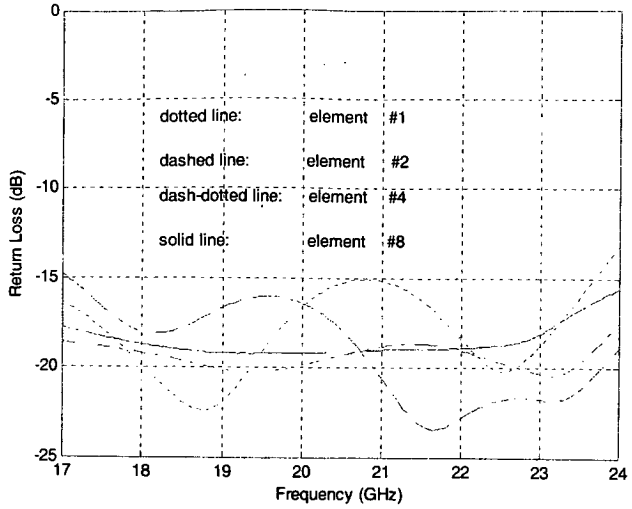

Figure 7 Return losses of elements 1, 2, 4, and 8 when all elements are uniformly excited simultaneously

2)th elements. From the results shown in the figure, one can make the following observations:

1. when only a single element is excited in the E-plane array, its return loss is degraded comparing with the return loss of the stand-alone element in Figure 4, especially in the middle of the band, but it is still less than -10 dB;
2. the return loss of the 1st element has fewer changes than that of the middle elements (the 4th and 8th elements), because the interference from adjacent elements to the edge-element only comes from single side, while the middle elements receive disturbances from both side elements;
3. the maximum coupling between adjacent elements is less than -20 dB;
4. the nonedge elements have almost same return loss because these elements basically have same environment and weak couplings between the adjacent elements;
5. for those elements away from the edges of the array, at around 18.9 GHz, couplings from the i^{th} element to the $(i \pm 1)^{th}$ elements have a deep notch; however, couplings from the i^{th} element to the $(i \pm 2)^{th}$ elements reach the maximum value at about 19.4 GHz.

After launching the Gaussian pulse at each individual element, the same pulse is launched at all the ports simultaneously with the same initial phase. The return loss RL_i at each port is calculated using

$$RL_i(f) = 20 \log_{10} \left| \frac{V_{i\,out}(f)}{V_{i\,inc}(f)} \right|, \qquad (2)$$

where $i = 1, 2, 3, \cdots 16$, and $V_{i\,out}$ is the output wave at the i^{th} port, which includes the reflected waves created by the discontinuities in the element and the coupled waves from other elements. Figure 7 plots the return losses at port 1, 2, 4, and 8. It is obvious that return loss is improved with respect to those shown in Figures 4 and 6. The improved return loss indicates that each element has a good impedance matching to its feeding line in the 16-element E-plane array, when the array is uniformly fed by a parallel feeding network. The calculated radiation patterns of the array are shown

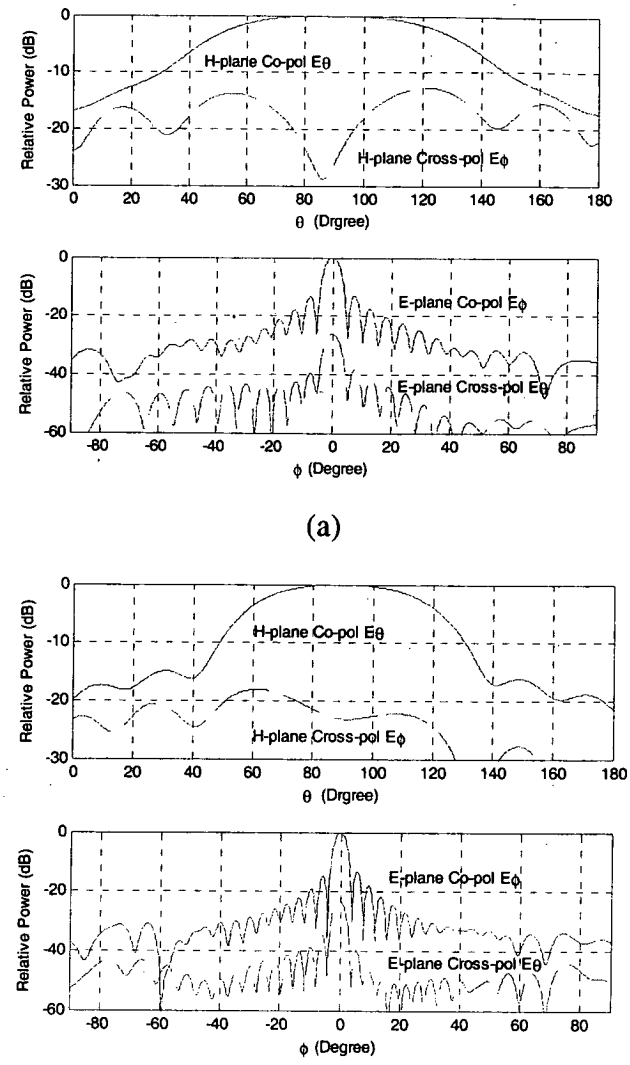

Figure 8 The simulated co-pol (solid line) and cross-pol (dashed line) patterns in the H-plane (X–Z) and E-plane (X–Y) at (a) 17.7 GHz and (b) 23.6 GHz

in Figure 8. The beamwidth at different radiation planes and different frequencies are summarized in Table 1.

4. THREE-PIECE ASSEMBLED PARALLEL-FED 16-ELEMENT LTSA ARRAY

To build the array studied in the previous section and to ensure that the air slab in the IML parallel feeding network is uniform, a three-piece assembled antenna structure has been created. Figure 9(a) illustrates the isometric drawings of three components and a portion of the assembled array. The components are as follows: the ground plate, which is an aluminum plate whose inside surface acts as the ground plane of the IML, and a number of spacers are

TABLE 1 Beamwidth (BW) of the 16-Element IML-Fed LTSA Array

Frequency	17.7 GHz	20.65 GHz	23.6 GHz
H-plane pattern BW	75.7°	64.3°	55.5°
E-plane pattern BW	4.8°	4.2°	3.7°

machined on top of the surface; the PCB, which holds the IML parallel feeding network, the IML-to-CPS transitions, and the LTSA elements; the metal cover, which can be an aluminum plate and has the same footprint as the ground plate. Grooves are machined inside the plate, and the pattern of the grooves is the same as the pattern of the spacers on ground plate. The depth of the grooves is 250 mil, which ensures that the cover does not change the performance of the IML FBN and IML-to-CPS transitions. The parallel feeding network and 16 elements printed on the PBC are shown in Figure 9(b). All the T-junctions are the same. There is a three-stage 100Ω-to-50Ω impedance transformer connected to the 100Ω-ports of the T-junction. When the three pieces are assembled together and held tightly by a number of screws, a uniform air slab is formed by the spacers, and the metal cover significantly reduces the radiation from the parallel-feeding network.

5. MEASURED RESULTS

An SMA connector is connected at the input port of BFN. The measured return loss of the array is given in Figure 10(a). The array has a good input impedance bandwidth from 17.7 to 23.6 GHz. The gain of the array is measured at six frequencies and plotted in Figure 10(b). The gain is about 0.5-dB less than the calculated array directivity [7], which designates that the array has a good efficiency. This is because (i) each element in the array has a good impedance match to its feeding line, (ii) the loss in BFN is reduced by using IML, and (iii) the radiation from BFN is eliminated by the metal cover. Figure 11 shows the E-plane radiation patterns measured at 17.7 and 23.6 GHz. They agree well with the calculated patterns shown in Figure 8.

6. CONCLUSION

An IML-fed LTSA element and its 16-element E-plane LTSA array have been designed using the FDTD method. The return losses and couplings in the 16-element E-plane linear array were studied numerically, with each element is excited individually. The calculated results show that the coupling between adjacent elements is less than −20 dB and the return loss can become worse than that of the standalone element. When the 16 elements are uniformly excited, the return loss of each element is better than that of the standalone element. The 16-element array was built using a new three-piece assembled antenna structure, and was fed by the IML parallel-feeding network. The measured results demonstrate that the array has a good impedance bandwidth and high antenna efficiency from 17.7 to 23.6 GHz.

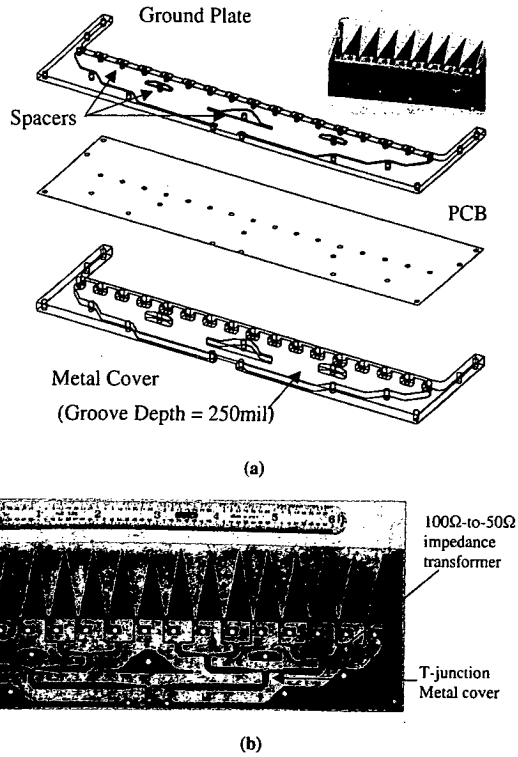

Figure 9 The three components used to build the 16-element IML-fed LTSA: (a) isometric view; (b) the BFN and elements on the PCB

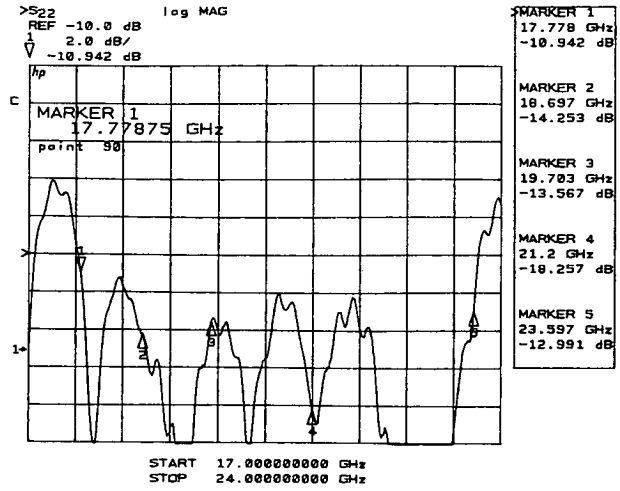

Figure 10 Measured (a) return loss and (b) gain of the 16-element IML-fed LTSA array

ACKNOWLEDGMENTS

The author would like to thank Dr. Jim P. Y. Lee and Dr. Pierre Lavoie of Defence R&D Canada—Ottawa, and Dr. John Litva of TenXc Inc., Ottawa, Canada, for their encouragement and great support.

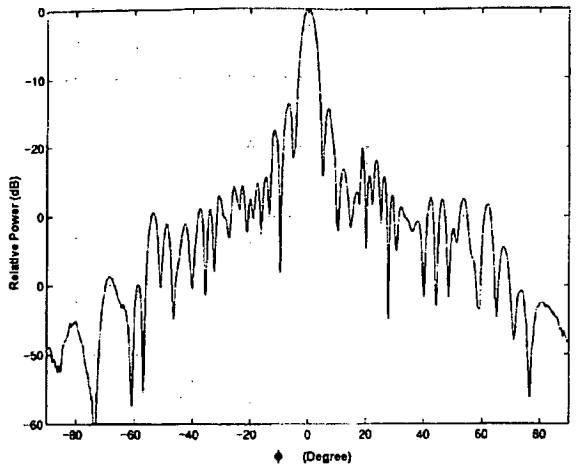

(a)

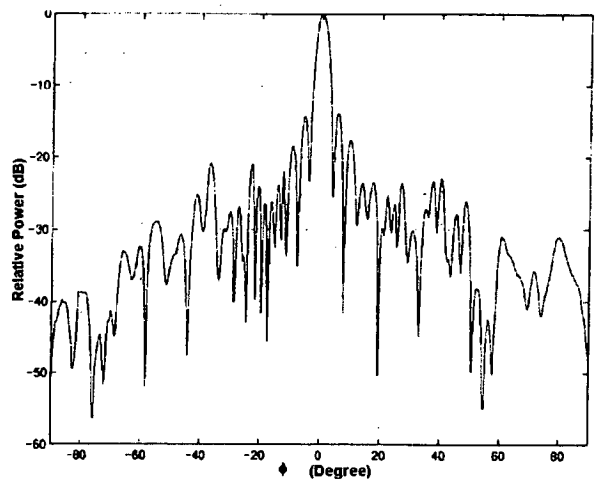

(b)

Figure 11 Measured E-plane patterns at (a) 17.7 GHz and (b) 23.6 GHz

REFERENCES

1. P.S. Kooi, T.S. Yeo, and M.S. Leong, Parametric studies of the linearly tapered slot antenna (LTSA), Microwave Opt Technol Lett 4 (1991), 200–207.
2. R.Q. Lee and R.N. Simons, Linearly tapered slot antenna and feed networks, Antenna Applic Symp, 1994.
3. P. Pramanick and P. Bhartia, Computer-aided design models for millimeter-wave fin lines and suspended substrate microstrip lines, IEEE Trans Microwave Theory Tech MTT-33 (1985), 1429–1435.
4. C. Wu, A K-band suspended microstrip line fed linear tapered slot antenna and its E-plane arrays, Microwave Opt Technol Lett 41 (2004), 451–455.
5. B.C. Wadell, Transmission-line design handbook, Artech House, Norwood, MA, 1991.
6. R.Q. Lee, Notch antennas, NASA/TM—2004-213057, Glenn Research Center, Cleveland, OH, 2004.
7. C. Wu, Use of the finite difference time domain method to study broadband antennas for millimeter wave point-to-point and point-to-multipoint communications, Ph.D. dissertation, McMaster University, Hamilton, Ontario, Canada, 2000.

TEMPERATURE DEPENDENCE OF LIGHT POLARIZATION IN ACTIVE ERBIUM-DOPED FIBER

M. A. Quintela,[1] F. J. Madruga,[1] M. López-Amo,[2] and J. M. López-Higuera[1]
[1] Photonics Engineering Group
Universidad of Cantabria, ETSIIT
Avda. Los Castros s/n
39005 Santander, Spain
[2] Departamento de Ingeniería Eléctrica y Electrónica
Universidad Pública de Navarra
Campus de Arrosadía s/n
31006 Pamplona, Spain

Received 11 October 2004

ABSTRACT: *Experimental results on the temperature dependence of the polarization state of the amplified optical signal between 0°C and 50°C are reported in this paper for an erbium-doped fiber amplifier. The instabilities of the polarization state decrease with increasing temperature when pumped at 1480 nm. The rates are reported.* © 2005 Wiley Periodicals, Inc. Microwave Opt Technol Lett 45: 246–249, 2005; Published online in Wiley InterScience (www.interscience.wiley.com). DOI 10.1002/mop.20785

Key words: *polarization; erbium-doped fiber; temperature; polarization variance; signal wavelength; input-signal power*

1. INTRODUCTION

The temperature dependence of the performance of erbium-doped fiber (EDF) is a key aspect for practical applications of the optical fiber amplifier. Therefore, this topic has been extensively studied [1–5]. These results reported in these studies concern the temperature dependence of the gain, amplified spontaneous emission (ASE), noise figure, and pump wavelength.

The gain and ASE decrease with increasing temperature [1, 3]. This behavior has been explained by the temperature dependence of the absorption σ_a and emission σ_e cross-section spectra, upon which the gain and the ASE characteristics are based.

In the trivalent erbium ion, the Stark effect removes the degeneracy, the ground, and the metastable energy, thus creating many sublevels. The populations of these sublevels follow Boltzman's law. σ_a and σ_e are closely related to the distribution of ions in the ground and metastable energy levels at a given temperature. EDF temperature changes are followed by a thermal distribution of the populations within of these sublevels and, as a consequence, the values of $\sigma_a(\lambda)$ and $\sigma_e(\lambda)$ are altered. For example, the decrease in temperature induces the lower components of the ground and metastable energy level to become highly populated. Thus, absorption at long wavelengths and fluorescence at short wavelengths decrease.

Furthermore, the gain change with temperature depends strongly on the pump wavelengths [4, 5]. When pumped at 1.48 μm, the performance of the EDF is more sensitive to temperature than when pumped at 0.5145, 0.66, 0.8, or 0.98 μm. This behavior is due to a combination of the proximity of the pump and signal energies and the temperature-dependent distribution of ions within the metastable and ground levels.

The polarization state (PS) of light in an erbium-doped fiber amplifier (EDFA) is also of importance in both the optical-communications [6] and photonic-sensing [7] fields. To quantify the instabilities and dependencies of the PS, the variance of the PS has been defined as a representative parameter [8, 9]. PS variance dependencies with regard to signal spectrum, pump power, and